NASA/TM—2003-212226

A Reduced Model for Prediction of Thermal and Rotational Effects on Turbine Tip Clearance

Javier A. Kypuros
University of Texas, Pan American University, Edinburg, Texas

Kevin J. Melcher
Glenn Research Center, Cleveland, Ohio

March 2003

The NASA STI Program Office . . . in Profile

Since its founding, NASA has been dedicated to the advancement of aeronautics and space science. The NASA Scientific and Technical Information (STI) Program Office plays a key part in helping NASA maintain this important role.

The NASA STI Program Office is operated by Langley Research Center, the Lead Center for NASA's scientific and technical information. The NASA STI Program Office provides access to the NASA STI Database, the largest collection of aeronautical and space science STI in the world. The Program Office is also NASA's institutional mechanism for disseminating the results of its research and development activities. These results are published by NASA in the NASA STI Report Series, which includes the following report types:

- TECHNICAL PUBLICATION. Reports of completed research or a major significant phase of research that present the results of NASA programs and include extensive data or theoretical analysis. Includes compilations of significant scientific and technical data and information deemed to be of continuing reference value. NASA's counterpart of peer-reviewed formal professional papers but has less stringent limitations on manuscript length and extent of graphic presentations.

- TECHNICAL MEMORANDUM. Scientific and technical findings that are preliminary or of specialized interest, e.g., quick release reports, working papers, and bibliographies that contain minimal annotation. Does not contain extensive analysis.

- CONTRACTOR REPORT. Scientific and technical findings by NASA-sponsored contractors and grantees.

- CONFERENCE PUBLICATION. Collected papers from scientific and technical conferences, symposia, seminars, or other meetings sponsored or cosponsored by NASA.

- SPECIAL PUBLICATION. Scientific, technical, or historical information from NASA programs, projects, and missions, often concerned with subjects having substantial public interest.

- TECHNICAL TRANSLATION. English-language translations of foreign scientific and technical material pertinent to NASA's mission.

Specialized services that complement the STI Program Office's diverse offerings include creating custom thesauri, building customized databases, organizing and publishing research results . . . even providing videos.

For more information about the NASA STI Program Office, see the following:

- Access the NASA STI Program Home Page at ***http://www.sti.nasa.gov***

- E-mail your question via the Internet to help@sti.nasa.gov

- Fax your question to the NASA Access Help Desk at 301–621–0134

- Telephone the NASA Access Help Desk at 301–621–0390

- Write to:
  NASA Access Help Desk
  NASA Center for AeroSpace Information
  7121 Standard Drive
  Hanover, MD 21076

NASA/TM—2003-212226

A Reduced Model for Prediction of Thermal and Rotational Effects on Turbine Tip Clearance

Javier A. Kypuros
University of Texas, Pan American University, Edinburg, Texas

Kevin J. Melcher
Glenn Research Center, Cleveland, Ohio

National Aeronautics and
Space Administration

Glenn Research Center

March 2003

This report contains preliminary findings, subject to revision as analysis proceeds.

The Propulsion and Power Program at
NASA Glenn Research Center sponsored this work.

Available from

NASA Center for Aerospace Information
7121 Standard Drive
Hanover, MD 21076

National Technical Information Service
5285 Port Royal Road
Springfield, VA 22100

Available electronically at http://gltrs.grc.nasa.gov

A Reduced Model for the Prediction of Thermal and Rotational Effects on Turbine Tip Clearance

Javier A. Kypuros
University of Texas, Pan American University
Edinburg, Texas 78539

Kevin J. Melcher
National Aeronautics and Space Administration
Glenn Research Center
Cleveland, Ohio 44135

Abstract

This paper describes a dynamic model that was developed to predict changes in turbine tip clearance – the radial distance between the end of a turbine blade and the abradable tip seal. The clearance is estimated by using a first principles approach to model the thermal and mechanical effects of engine operating conditions on the turbine subcomponents. These effects are summed to determine the resulting clearance. The model is demonstrated via a ground idle to maximum power transient and a lapse-rate takeoff transient. Results show the model demonstrates the expected "pinch point" behavior. The paper concludes by identifying knowledge gaps and suggesting additional research to improve the model.

Nomenclature

Symbol	Units	Description
A	m^2	area
E	Pa	Young's modulus
F	N	force
L	m	unstressed blade length
N	RPM	rotational speed
P	Pa	pressure
T	°C	temperature
V	m^3	volume
c	J/kg-°C	specific heat
h	W/m^2-°C	convection heat transfer coefficient
k	W/m-°C	thermal conductivity
l	m	stressed blade length
q	W	heat transfer rate
r	m	radius
t	sec	time
u	m	deformation
w	m	width
α	1/°C	thermal expansion coefficient
δ		tip clearance
ρ	kg/m^3	density
ν		Poisson's ratio
ω	rad/sec	angular speed
σ	Pa	stress
ε	m/m	strain
η		film cooling effectiveness
π		ratio of the perimeter of a circle to its diameter

1. Introduction

Turbine blade tip clearance continues to be a concern in the design and control of gas turbines. Ever increasing demands for improved efficiency and higher operating temperatures require more stringent tolerances on turbine tip clearance. A successfully implemented active tip clearance control is expected to have benefits of increased efficiency, reduced specific fuel consumption, and additional service life.

The focus of this study is to develop a simplified model from first principles that grossly captures the dynamic change in turbine tip clearance during take-off. Such a model can aid in identifying and understanding the primary mechanisms involved in the turbine tip clearance problem and their inherent frequency response. This work serves to identify knowledge gaps that must be addressed in order to facilitate design and development of an actuator and control strategy for active clearance control. Furthermore, this work is a step towards a higher fidelity model suitable for *virtual prototyping*[*] of a controller/actuation mechanism. The purpose of beginning with this first-principles approach is to eliminate the necessity for a finite-element model that would require detailed information about geometry specific to a particular engine system. The model developed herein is intended to be more generic.

The main objectives of this study can be summarized as follows:

1. Identify and characterize the primary mechanisms involved in turbine tip clearance dynamics;
2. Identify the known and unknown parameters necessary to predict turbine tip clearance; and
3. Develop a simplified model that can be used to:
   (a) reasonably represent turbine tip clearance during common gas turbine transients (take-off, reburst, etc.),
   (b) determine actuator performance requirements for active clearance control, and
   (c) serve as a baseline for virtual prototyping of a controller and actuation system.

Previous NASA efforts in collaboration with industry have quantified tip clearance transients using both experimental and numerical results [1, 2, 3]. One example is the Energy Efficient Engine studies [1] conducted in the late 1970's and early 1980's. Under these studies, detailed analyses and experiments were performed to identify the dynamic characteristics of mechanisms impacting turbine tip clearance. Due to proprietary issues, these reports, however, do not describe analysis used to derive numerical results. Much of this work has been reserved for classified reports which document analyses performed using proprietary finite-element tools, and few publications document the combined effects of both thermal and mechanical stresses experienced by the rotor, blade, and shroud. Little has been published on the stress analysis used to predict deflections of the rotor, blade, or shroud. Most of the finite-element studies in the area focus on long term effects like creep and crack propagation and do not focus on prediction of deflections due to thermal and rotational transients during flight. Significant experimental and numerical work has been published on the film cooling of turbine blades [4, 5, 6, 7, 8]. For NASA to conduct fundamental research that will facilitate future technologies in active turbine tip clearance control, a valid model or a test rig is necessary. The test rig can be potentially costly to build and run. A model-based simulation is less costly, and is useful in designing the test rig and associated experiments. If sufficiently accurate, it can be used to virtually prototype the controller/actuator mechanism.

This document is divided into four chapters, introduction, model development, implementation and results, and discussion. The section on model development is presented in three sub-sections based on the three system elements composing the turbine – the shroud, rotor, and blade. Each element is presented by describing the parameters and boundary conditions necessary for analysis and by detailing assumptions used to facilitate results. Analyses used to determine thermal and mechanical deflections are described for each element. This is followed by a section in which parameter values are defined for simulation purposes; and preliminary results of clearance predictions are presented and discussed. The

[*] *Virtual prototyping* refers to the process by which models and simulations are employed to *virtually* design and test mechanisms and/or controls.

paper concludes with a discussion in which the knowledge gaps of most concern are identified and summarized, and suggestions for further model development are presented.

2. Model Development

As shown in Figure 1, the proposed model incorporates three basic elements – the shroud, turbine rotor (or disk), and turbine blade. In order to predict deflections of each element due to thermal and mechanical stresses the temperature, pressure, and force distributions in each element must be modeled. The block diagram shows the parameters necessary to calculate these temperature and stress distributions. An engine model, not discussed in this report, is employed to provide speed, temperature, and pressure transients for the shroud, rotor, and blade sub-models. Each sub-model predicts deflections due to thermal and mechanical stresses. As shown in Equation 1, the relative change in the time-varying geometry of each sub-model is then used to calculate the overall change in tip clearance.

$$\begin{aligned}\delta(t) &= r_{shroud}(t) - \left[r_{rotor}(t) + l_{blade}(t)\right] \\ &= (r_a + u_{s1} + u_{s2}) - \left[(r_0 + u_{r1} + u_{r2}) + (L + u_{b1} + u_{b2})\right]\end{aligned} \tag{1}$$

Here, $r_{shroud}(t)$, $r_{rotor}(t)$, and $l_{blade}(t)$ are, respectively, the shroud inner radius, rotor outer radius, and blade length as a function of time. Note that, r_a, r_0, and L are the initial geometric state of the shroud, rotor, and blade respectively; while the subscripted u's denote deformations due to thermal and mechanical forces.

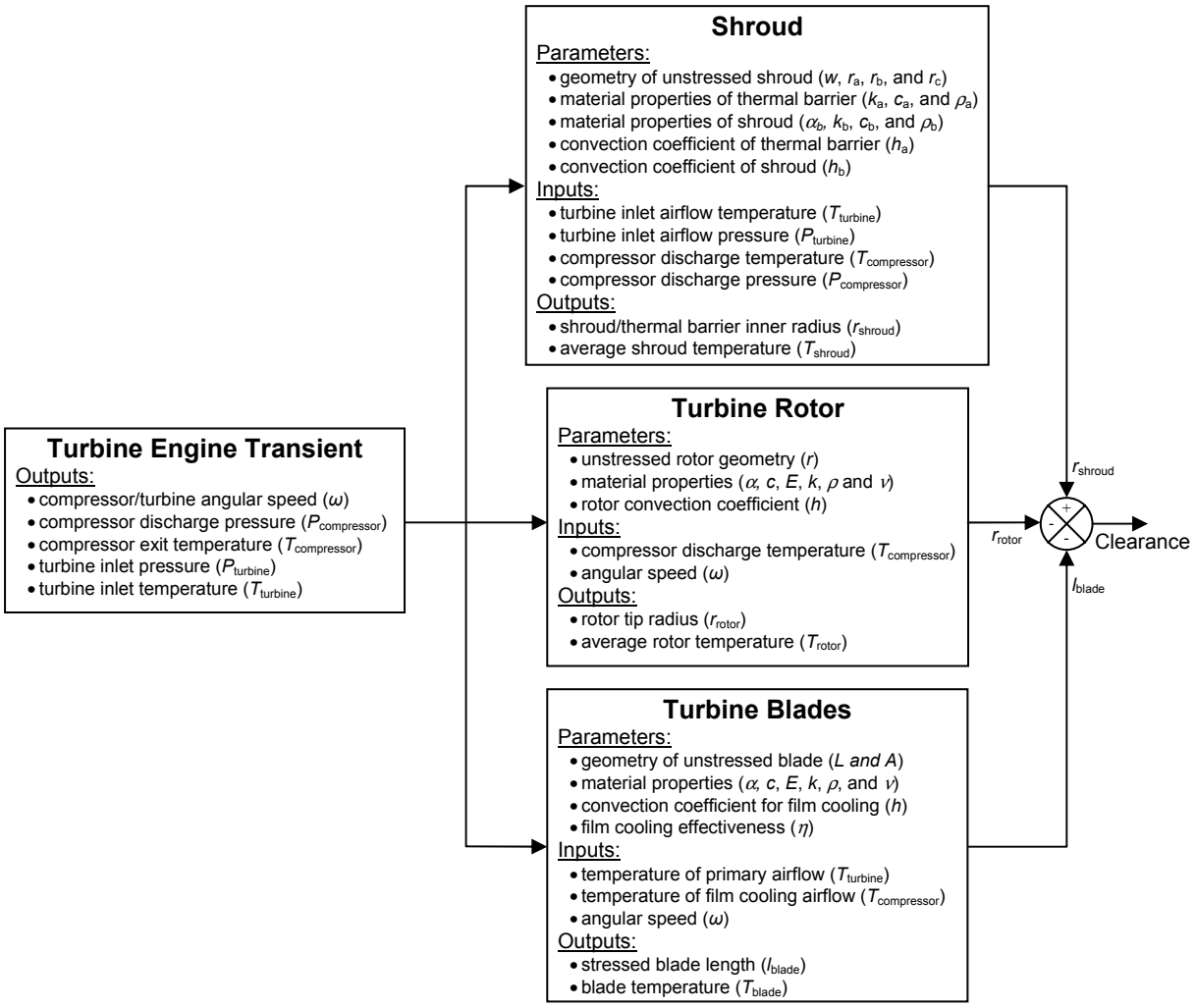

Figure 1. Block diagram for tip clearance model

Equations for calculating these deflections will be given in the subsections that follow.

2.1. Shroud

As shown in Figure 2, it is assumed that the general geometry of the shroud is a ring-like structure where the inner surface is coated with an abradable material that also functions as a thermal barrier. However, the shroud is not a single continuous ring-like structure. Instead it is made up of a series of arcs joined together to form a ring, which may negate the usefulness of this assumption. This issue shall be addressed in § 2.1.4 with an alternative formulation of the shroud growth due to thermal stresses on the casing to which the shroud is attached. The inner surface of the abradable material at radius r_a is exposed to heated gas at a temperature approximately equal to the turbine inlet temperature, $T_{turbine}$. The outer surface of the shroud at radius r_b is exposed to compressor discharge air which is assumed to be at the compressor discharge temperature, $T_{compressor}$. As shown in Figure 2, pressure distributions on the inner and outer surface of the shroud are adapted from Lattime and Steinetz [9]. For simplicity, pressure in the tip clearance region is assumed to vary linearly between the turbine inlet and exit pressures. Compressor bleed air is used to purge the space between the shroud and the casing. To facilitate results, it is assumed that the temperature difference between the compressor discharge and the shroud outer surface is negligible.

For the purposes of this study, the abradable material is presumed to function primarily as a thermal barrier and not as a structural member. It is assumed, therefore, that the abradable material acts as a coating and does not impose a significant stress on the inner surface of the superalloy layer as the shroud grows due to thermal loads. Additionally, because the shroud is attached to the case in the form of a series of arcs, it is assumed that the abradable material layer maintains its approximate thickness even when thermally stressed (i.e. the relative distance between the bond radius and inner wall, r_c–r_a, is

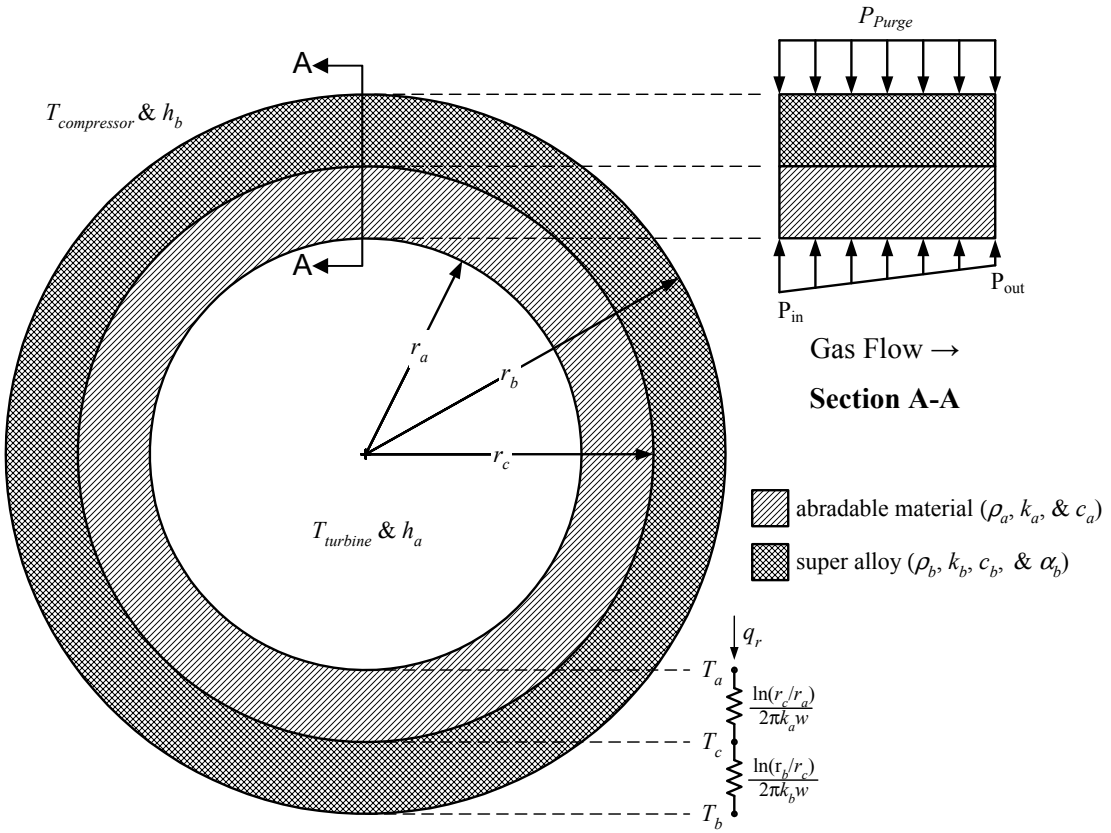

Figure 2. Shroud schematic

assumed to remain relatively constant). Due to its conductive properties, the abradable layer dissipates much of the turbine heat, thus reducing the temperature otherwise experienced by the superalloy surface at radius r_c. This temperature, T_c, is the thermal boundary condition on the inner surface of the alloy used to calculate the deflection due to thermal stresses. The heat transfer at the inner surface of the abradable material and outer surface of the alloy are assumed to be uniform (quasi-steady) to facilitate a simple model. Heat is convected to the inner surface of the abradable material at wall temperature T_a with a heat transfer coefficient of h_a. The convection coefficient at the outer surface of the shroud is h_b and the associated surface temperature is T_b.

2.1.1. Shroud Heat Transfer

To facilitate a closed form solution for the heat transfer across the shroud, the responses near the shroud surfaces are assumed to be governed by a semi-infinite formulation of the transient heat conduction equation where the temperature at the surface, T_w, is given by the classical solution [6, 7]:

$$\frac{T_w - T_i}{T_r - T_i} = 1 - \exp\left[\frac{h^2}{\rho c k} t\right] \operatorname{erfc}\left[\frac{h}{\sqrt{\rho c k}} t\right] \tag{2}$$

where T_r and T_i are the reference temperature and initial wall temperature, respectively. This formulation is appropriate as long as the transient temperature penetration does not exceed the thickness of the wall material.* For a single-flow system, the reference temperature is the temperature of the mainstream flow which for the inner surface of the shroud is assumed to be $T_{turbine}$ and for the outer surface $T_{compressor}$. This formulation is used to calculate the inner and outer shroud wall temperatures, T_a and T_b, respectively.

Using a thermal resistance formulation [10] as shown in Figure 2, one can estimate the bond temperature, T_c, at the interface between the abradable material and the superalloy:

$$\frac{T_a - T_b}{\frac{\ln(r_c / r_a)}{2\pi k_a w} + \frac{\ln(r_b / r_c)}{2\pi k_b w}} = \frac{T_a - T_c}{\frac{\ln(r_c / r_a)}{2\pi k_a w}} \quad \Rightarrow \quad T_c = T_a - \frac{T_a - T_b}{1 + \frac{\ln(r_b / r_c)}{\ln(r_c / r_a)} \frac{k_a}{k_b}}. \tag{3}$$

Additionally, by representing the superalloy layer of the shroud as a hollow cylinder and assuming one-dimensional heat conduction in the radial direction under quasi-steady state conditions, the heat diffusion equation simplifies to

$$\frac{1}{r} \frac{d}{dr}\left(kr \frac{dT}{dr}\right) = 0$$

which, when integrated and combined with the boundary conditions $T(r_c)=T_c$ and $T(r_b)=T_b$, results in the radial temperature distribution

$$T(r) = T_c + (T_b - T_c) \frac{\ln(r / r_c)}{\ln(r_b / r_c)}. \tag{4}$$

2.1.2. Shroud Deflection due to Thermal Stresses, u_{s1}

To enable prediction of shroud deflection due to thermal stresses, it is assumed that the stresses and displacement do not vary over the width of the shroud. The formulation presented herein is equivalent to that given in [11] for a thin circular disk with a hollow center (like a ring). According to Timoshenko [11], the radial and tangential stresses (σ_r and σ_θ) must satisfy the equation of equilibrium

$$\frac{d\sigma_r}{dr} + \frac{\sigma_r - \sigma_\theta}{r} = 0 \tag{5}$$

*The application of the semi-infinite solution should be justified in future work and is used here primarily to facilitate initial results.

The strain components in the radial and tangential directions are

$$\varepsilon_r = \alpha T + \frac{1}{E}(\sigma_r - \nu\sigma_\theta) = \frac{du}{dr}$$

and

$$\varepsilon_\theta = \alpha T + \frac{1}{E}(\sigma_\theta - \nu\sigma_r) = \frac{u}{r}$$

The above strain equations can be solved for the radial and tangential stresses:

$$\sigma_r = \frac{E}{1-\nu^2}\left[\varepsilon_r + \nu\varepsilon_\theta - (1+\nu)\alpha T\right]$$

and

$$\sigma_\theta = \frac{E}{1-\nu^2}\left[\varepsilon_\theta + \nu\varepsilon_r - (1+\nu)\alpha T\right]$$

Given the above stress equations and noting that $\varepsilon_r = du/dr$ and $\varepsilon_\theta = u/r$ the equilibrium equation (Equation 5) may be written as

$$\frac{d}{dr}\left[\frac{1}{r}\frac{d(ru)}{dr}\right] = (1+\nu)\alpha\frac{dT}{dr}.$$

Integrating twice yields the radial deflection

$$u(r) = (1+\nu)\alpha\frac{1}{r}\int_{r_c}^{r} Tr\,dr + C_1 r + \frac{C_2}{r} \tag{6}$$

where r_c is the lower limit of the radius or in this case the unstressed inner wall radius of the shroud superalloy layer. Assuming no thermal stress at the inner and outer boundaries of the superalloy portion of the shroud (surfaces stresses due to pressure will be considered separately in § 2.1.3) and recalling the radial temperature distribution (Equation 4), C_1 and C_2 are:

$$C_1 = \frac{\alpha(1-\nu)}{2}\left[T_c + \left(\frac{r_b^{\,2}}{r_b^{\,2} - r_c^2} - \frac{1}{2\ln(r_b/r_c)}\right)(T_b - T_c)\right] \tag{7}$$

and

$$C_2 = \frac{\alpha(1+\nu)r_c^2}{2}\left[T_c + \left(\frac{r_b^{\,2}}{r_b^{\,2} - r_c^2} - \frac{1}{2\ln(r_b/r_c)}\right)(T_b - T_c)\right]. \tag{8}$$

Because the abradable material is thought to serve mainly as a thermal barrier, the shroud deflection is primarily due to the superalloy layer and thus should be measured from the unstressed bond radius, r_c. The thickness of the abradable material layer can later be subtracted since, as previously mentioned, it is assumed to remain relatively constant. Thus the shroud radial deflection due to thermal stresses is

$$u_{s1} = u(r_c) = \alpha r_c\left[T_c + \left(\frac{r_b^{\,2}}{r_b^{\,2} - r_c^{\,2}} - \frac{1}{2\ln(r_b/r_c)}\right)(T_b - T_c)\right]. \tag{9}$$

2.1.3. Shroud Deflection due to Pressure Differential, u_{s2}

To predict deflection of the shroud at the bond radius, r_c, due to pressure differential, Timoshenko's hollow cylinder equation is adapted [11]:

$$u_{s2} = \frac{1}{E(r_b^{\,2} - r_c^2)}\left[(1-\nu)r_c(P_i r_c^2 - P_o r_b^{\,2}) - (1+\nu)r_c r_b^{\,2}(P_o - P_i)\right]. \tag{10}$$

In Equation 10, P_i is the mean internal pressure and P_o is the outer surface pressure. Per Figure 2, they are equivalent to $(P_{in} + P_{out})/2$ and P_{purge}, respectively.

2.1.4. Alternative Shroud Growth Formulation

Alternatively, the deflection of the shroud can be thought of as limited by the casing growth. The shroud can be then modeled as a series of arcs rigidly attached to the casing as shown in Figure 3. The casing grows due to thermal and pressure differentials. Similar to the previous formulation, the surface temperatures on the outer and inner surfaces of the casing, T_e and T_d, can be calculated from mainstream flow temperatures and experimentally or numerically determined convection coefficients using Equation 2. The outer casing wall, r_e, is assumed to be exposed to ambient temperature and pressure (T_∞ and P_∞). If the casing is grossly modeled as a hoop-like structure then deflection due to thermal differential can be derived as was done in § 2.1.2. The deflection due to thermal stresses would, alternatively, be as shown in Equation 11.

$$u_{s1} = \alpha r_d \left[T_d + \left(\frac{r_e^{\,2}}{r_e^{\,2} - r_d^{\,2}} - \frac{1}{2\ln(r_e / r_d)} \right) (T_e - T_d) \right]. \tag{11}$$

Similarly, the alternative deflection due to pressure differential can be derived as

$$u_{s2} = \frac{1}{E(r_e^{\,2} - r_d^{\,2})} \left[(1-\nu) r_d (P_i r_d^2 - P_o r_e^{\,2}) - (1+\nu) r_d r_e^{\,2} (P_o - P_i) \right]. \tag{12}$$

where P_i is now the pressure inside the cavity, P_{purge}, and P_o is the ambient pressure, P_∞.

In this model, a higher bandwidth mechanical clearance control system is presumed to replace the slower thermal clearance control systems found on many current commercial engines. Therefore, active cooling of the case is not considered. The deformation of the structure that connects the shroud to the case is another effect that is not developed here. The structure deforms as the differential pressure across the shroud changes, and so, should be included in the alternative formulation.

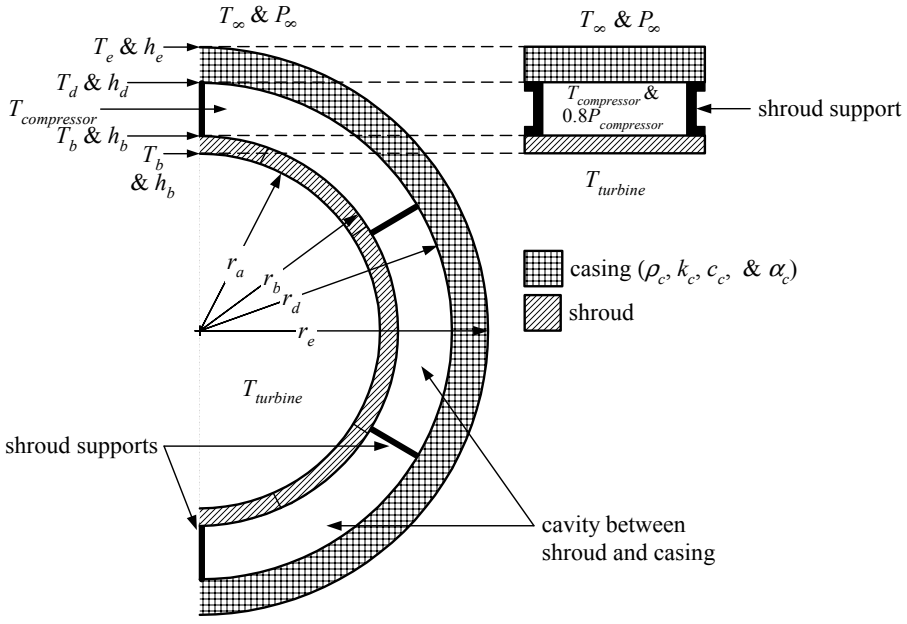

Figure 3. Shroud/casing schematic

2.2. Rotor

Detailed studies of rotor-stator systems have been conducted by Owen [12]. However, in the attempt to arrive at a simplified model representing the gross clearance dynamics, this initial effort has focused on modeling the first-order effects. For this initial study, the rotor structure is modeled as a rotating disk of uniform thickness, and only deflections due to changes in centrifugal forces and purge air temperature are considered. Compressor discharge air is generally used to purge and cool the cavity around the rotor. Only the small tip surface of the rotor is exposed to the high temperature core flow. Thermal expansion is assumed to be dominated by heat transfer between the rotor disk and the compressor discharge air, at temperature $T_{compressor}$. Thus, as suggested by Figure 4, the rotor is assumed to be insulated to heat transfer from the turbine blades simplifying the analysis. Compressor discharge air flows over the majority of the rotor's surface area.

2.2.1. Rotor Deflection due to Thermal Stresses, u_{r1}

As with the outer shroud surface temperature, the rotor surface temperature is assumed to be governed by the semi-infinite formulation (i.e., Equation 2) where the reference temperature is the compressor discharge temperature. Because most of the rotor's surface is exposed to the discharge temperature, the temperature through the width of the rotor is assumed to be relatively constant across the surface and approximately equal to the surface temperature (i.e., $T_{rotor}=T_{compressor}$). Note that in this simplified model, windage heating, which may produce a significant temperature gradient between the hub and the tip, is ignored.

As with the outer shroud surface, the heat transfer convection coefficient is not known, but it is assumed to be similar in magnitude to that given for the inner shroud surface. Since the rotor temperature is assumed to be relatively constant throughout, the thermal strain analysis is significantly simplified:

$$\varepsilon_r = \alpha T = \frac{du}{dr} \text{ and } \varepsilon_\theta = \alpha T = \frac{u}{r}.$$

Therefore, the approximate rotor deflection due to thermal stresses is

$$u_{r1} = \alpha T r_0 \tag{13}$$

where α_r and r_0 are the rotor thermal expansion coefficient and unstressed radius, respectively.

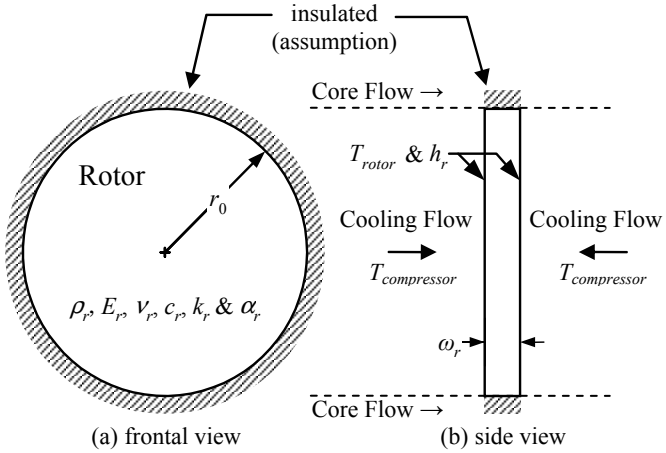

Figure 4. Rotor schematic

2.2.2. Rotor Deflection due to Centrifugal Forces, u_{r2}

To estimate the rotor tip radial deflection due to centrifugal forces, a simplified form of the rotating flat disk equation from reference 11 is used:

$$u_{r2} = \frac{1}{4E}(1-\nu_r)\rho_r\omega^2 r_0^{\ 3} \tag{14}$$

where ν_r, ρ_r, and E_r are material properties and $\omega=(2\pi/60)N$ is the rotor angular speed in rad/sec.

2.3. Blades

Of the three basic components, the most documented is the turbine blade. The blades are stressed by both centrifugal forces and thermal expansion. Because of the high temperatures within the turbine stage the turbine blades are film cooled by compressor discharge air. As shown in Figure 5, compressor discharge air that flows through the blade exits film cooling holes on the leading edge of the blade and is introduced into the boundary layer at the surface of the blade. The blades are of length L and cross-sectional area A_c.

2.3.1. Film Cooling of Turbine Blades

Film cooling is employed to reduce the heat transfer from hot air in the turbine at the turbine inlet temperature, $T_{turbine}$, to prevent surface temperatures in excess of the blade material's melting point. In film cooling, a secondary flow is introduced into the boundary layer at the surface of the blade [13]. The temperature of the film cooling fluid, T_f, is much lower than the mainstream temperature, T_m. The blade surface temperature, T_{blade}, is determined using a semi-infinite formulation similar to Equation 2 with the exception that the reference temperature, T_r, is not the mainstream temperature as in two temperature flows. The reference temperature for film cooling is generally unknown and depends on the supply temperatures of the two interacting flows and the degree of mixing that occurs [6, 7]. In such cases, the reference temperature and convection coefficient, h, must be determined experimentally or numerically. Using experimental data, a film cooling effectiveness, similar to that shown in Equation 15, is determined in terms of the two flow temperatures, T_m and T_f [7].

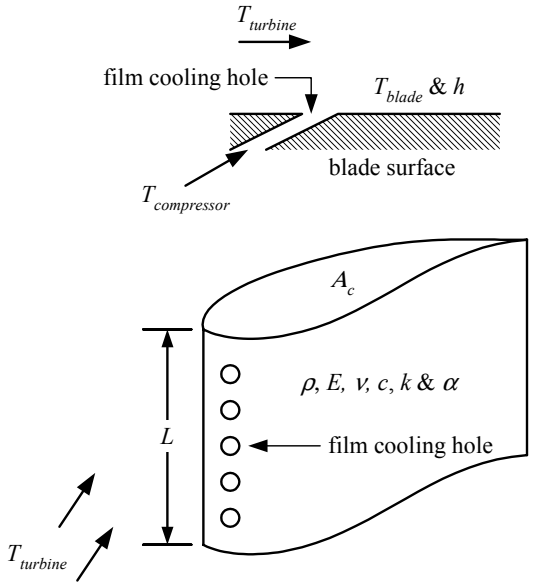

Figure 5. Blade schematic

$$\eta = \frac{T_r - T_m}{T_f - T_m}. \tag{15}$$

In the case of the turbine blades, the mainstream fluid is at $T_{turbine}$ and the film cooling flow is assumed to be at the compressor discharge temperature, $T_{compressor}$.

2.3.2. Blade Deflection due to Thermal Stresses, u_{b1}

The blade is relatively thin, and thus the thermal gradient through the thickness of the blade is assumed negligible. Therefore, the blade is assumed to have a uniform temperature equal to the surface temperature, T_{blade}. This simplifies the thermal stress analysis and results in a simple linear relation:

$$u_{b1} = \alpha T L \,. \tag{16}$$

2.3.3. Blade Deflection due to Centrifugal Forces, u_{b2}

Like the rotor, the blade is stressed by centrifugal forces. To simplify results, the maximum blade and rotor growth are thought to be sufficiently small to assume that the centrifugal force, F_c, is primarily a function of the rotor's angular velocity, $\omega(t)$, and does not vary significantly due to the rotor and blade growth. The deflection can hence be determined from a simple stress strain relation:

$$\begin{aligned} \varepsilon = \frac{\sigma}{E} = \frac{F_c / A_c}{E} = \frac{m(L + r_0)\omega^2}{E A_c} = \frac{\rho L (L + r_0)\omega^2}{E} = \frac{\Delta L}{L} \\ \Rightarrow \quad u_{b2} = \Delta L = \frac{\rho L^2 (L + r)\omega^2}{E}. \end{aligned} \tag{17}$$

2.4. Clearance Calculation

Having obtained expressions for the time varying deflections of the various turbine sub-models due to thermal and mechanical forces, these can now be summed to obtain the resulting tip clearance. Equation 1, reproduced here for convenience, shows how the relative change in the time-varying geometry of each sub-model is used to calculate the overall change in tip clearance.

$$\begin{aligned} \delta(t) &= r_{shroud}(t) - \left[r_{rotor}(t) + l_{blade}(t) \right] \\ &= (r_a + u_{s1} + u_{s2}) - \left[(r_0 + u_{r1} + u_{r2}) + (L + u_{b1} + u_{b2}) \right] \end{aligned}$$

Here, $\delta(t)$ is the overall tip clearance as a function of time. Variables r_{shroud}, r_{rotor}, and l_{blade} are, respectively, the shroud inner radius, rotor outer radius, and blade length as a function of time. Note that, r_a, r_0, and L are the initial geometric state of the shroud, rotor, and blade, respectively; while the subscripted u's denote time-dependent results of previously described deformation calculations.

3. Model Implementation and Results

In this section specific parameters used in implementing a dynamic simulation containing the previously presented tip clearance model are discussed, along with results from that simulation. Details of the actual implementation are not given here, but are given in the Appendix included at the end of this report.

3.1. Implementation

In this section, values are given for the various parameters required to implement the tip clearance model described in this paper. The parameters include geometry, material properties, and heat transfer coefficients. A consistent set of data containing all of the necessary model parameters was unavailable. Therefore, it was necessary to use estimates for many of the parameters. What follows is a discussion of

the sources, confidence level, and associated assumptions used in determining the various parameter values.

3.1.1. Shroud

Pressure distributions on the inner and outer surface of the shroud as shown in Figure 2 are adapted from Lattime and Steinetz [9]. For simplicity, pressure in the tip clearance region is assumed to vary linearly between the turbine inlet and exit pressures. Per Lattime and Steinetz [9], these pressures are approximately 70% and 30% of compressor discharge, respectively. The resulting average pressure, $0.5P_{compressor}$, is used on the inner surface of the shroud to determine the shroud deflection due to pressure differential. Compressor bleed air is also used to purge the space between the shroud and the casing. The resultant pressure on the outer shroud surface is assumed to have an even distribution approximately 80% of $P_{compressor}$. In this preliminary model, delays between the pressure signal at the compressor exit and the subsequent signal in the turbine are assumed negligible.

The shroud parameters and material properties are given in Table 1. Subscript *a* denotes materials and surface conditions of the abradable material, while subscript *b* denotes the same for the superalloy. For the purposes of this model the superalloy layer is assumed to be made of Inconel 718 and the abradable material of a partially stabilized Zirconium Oxide. Parameter values are rated on a level of confidence from 1 to 5; 5 indicating near certainty. Experimental approximations of the convection coefficient on the inner surface of the shroud (i.e., in the tip clearance region) are given in [8] and match reported experimental results for the blade tip [4, 5, 6, 7]. The convection heat transfer coefficient for the outer surface of the shroud is not known at this time but to facilitate results is assumed to be similar in magnitude to that on the inner shroud surface.

For the alternative shroud growth formulation, the inner casing wall, r_d, is exposed to the compressor discharge temperature, $T_{compressor}$, and approximately 80% of the compressor discharge pressure, $0.8P_{compressor}$. Convection coefficients for the case are not readily available.

Table 1. Shroud parameters

Parameter	Description	Value	Confidence
r_a	thermal barrier inner radius	38 cm (~15 in)	4
r_b	shroud outer radius	38.6 cm (~15.2 in)	3
r_c	shroud inner (bond) radius	48.3 cm (~15.1 in)	3
w	shroud width	5.1 cm (~2 in)	4
ρ_a	abradable material density	5030 kg/m^3	3
k_a	abradable material thermal conductivity	2.93 W/m-°C	3
c_a	abradable material specific heat	456 J/Kg-°C	3
ρ_b	shroud density	8220 kg/m^3	5
k_b	shroud thermal conductivity	24.9 W/m-°C	5
c_b	shroud specific heat	645 J/Kg-°C	5
α_b	shroud thermal expansion coefficient at 538°C	15.1x10^{-6} 1/°C	5
h_a	convection coefficient at inner surface	500 W/m^2-°C	4
h_b	convection coefficient at outer surface	1000 W/m^2-°C	2

3.1.2. Rotor

Rotor disks in most modern gas turbines are fabricated using newer members of the René family of superalloys. Some rotors [1] are fabricated from René 95 which has properties similar to Inconel 718. For this work, properties of Inconel 718 are used. Table 2 gives parameters used in the rotor sub-model.

Table 2. Rotor parameters

Parameter	Description	Value	Confidence
r_0	unstressed radius	32.9 cm (~13 in)	3
w_r	width	5.1 cm (~2 in)	3
ρ_r	density	8220 kg/m^3	4
E_r	modulus of elasticity	139 GPa	4
ν_r	Poisson's ratio	0.4	4
k_r	thermal conductivity	24.9 W/m-°C	4
c_r	specific heat	645 J/Kg-°C	4
α_r	thermal expansion coefficient	15.1x10^{-6} 1/°C	4
h_r	convection coefficient at surface	500 W/m^2-°C	2

3.1.3. Blades

The blade parameters, material properties, and parameter confidence levels are given in Table 3. For this initial model, blades are assumed to be made of a material similar to Inconel 718. Turbine blades found in modern gas turbine engines are generally fabricated as single crystals using the René family of superalloys. The incorporation into the clearance model of properties for these superalloys would be appropriate for future studies.

Experimental values for both the convection coefficient and effectiveness are presented in [6, 7] and numerical estimations of the convection coefficient can be found in [14, 15]. For the purpose of this study, a bulk or blade-surface-averaged effectiveness and convection coefficient are used. Given the experimentally determined convection coefficient and effectiveness, Equations 2 and 15 can be used to determine the blade surface temperature, T_{blade}.

Table 3. Blade parameters

Parameter	Description	Value	Confidence
L	unstressed length	5 cm (~1.97 in)	3
A_c	cross-sectional area	6 cm^2 (~0.93 in^2)	3
ρ	density	8220 kg/m^3	5
E	modulus of elasticity	139 GPa	5
ν	Poisson's ratio	0.4	4
k	thermal conductivity	24.9 W/m-°C	5
c	specific heat	645 J/Kg-°C	5
α	thermal expansion coefficient at 871 °C	16.4x10^{-6} 1/°C	5
h	convection coefficient at surface	1000 W/m^2-°C	3
η	film cooling effectiveness	0.5	3

3.2. Results

In this section the transient clearance is predicted for a ground idle-to-maximum power transient and for a lapse-rate take-off transient. As shown in the upper plot of Figure 6, the ground-idle to maximum power transient consists of a step in the throttle setting between the two operating conditions. A lapse-rate take-off transient involves ramping the throttle setting from ground-idle to about 90% of maximum power, performance of final flight checks, and then ramping up to maximum power. The throttle transient for the lapse-rate takeoff is shown in the upper plot of Figure 8.

For the ground idle-to-maximum power transient, the time history of the engine speed is shown on the upper axes of Figure 6. Associated temperatures transients for the high pressure turbine and the

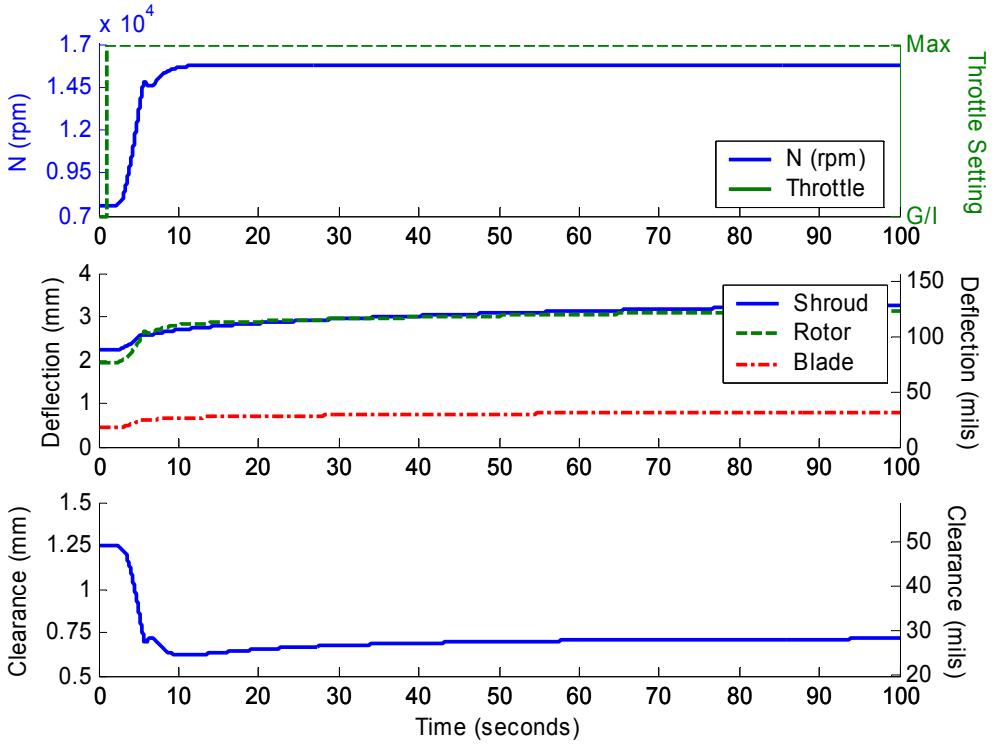

Figure 6. Deflections and clearance for transient from ground idle (G/I) to maximum power

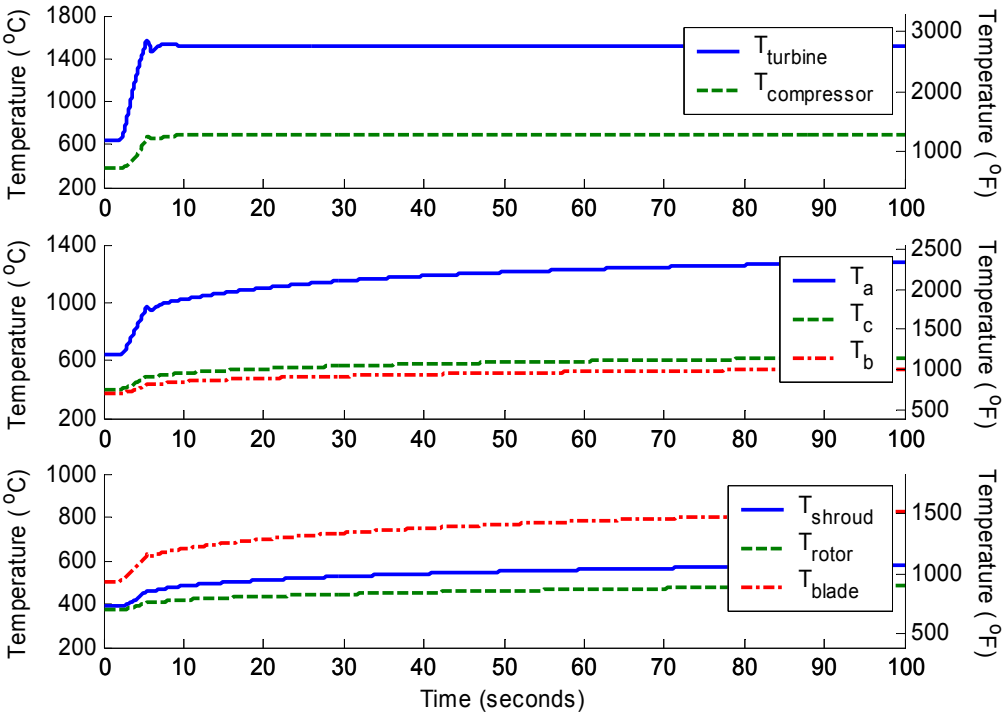

Figure 7. Temperatures for transient from ground idle (G/I) to maximum power

high pressure compressor are shown on the upper axes of Figure 7. Similar plots for the lapse-rate-take-off transient are shown on the upper axes of Figure 8 and Figure 9. Recall from Figure 1, that these parameters serve as inputs to the shroud, rotor, and blade sub-models. It is important to note that a transient simulation of a large commercial engine was not available. Instead, a simulation of a small military engine was used to generate the input transients. The transients were then scaled (as shown) to approximate the dynamics of a large commercial engine, for which the clearance model was developed.

In addition to the transient temperature inputs, Figure 7, shows the shroud temperatures and the basic element temperatures. Note that the shroud temperature, T_{shroud}, plotted on the lower axis, is just the average of the bond and outer wall temperatures, T_c and T_b, respectively. As evidenced by the figure, the dynamic temperatures generally follow the expected trend – a relatively slow response compared to the input temperature transients. The outer wall temperature approaches an expected steady-state value between 1200-1300 ˚F. However, the bond temperature does not appear to approach an expected value of near 1800 ˚F. This is likely due to three primary reasons:

1. the convection coefficient for the outer shroud surface is not known or well documented so the assumed value may be incorrect,
2. the actual properties of the abradable material are not known. A change in the thermal conductivity of the abradable material significantly affects the bond temperature, and
3. the input engine transients may not match those for a larger commercial engine.

Data on the lower axes also show that the blade wall temperature, T_{blade}, stays well below Inconel 718's melting point of 2370 ˚F.

Figure 6 shows the individual deflections and overall clearance with reference to the engine speed transient. As expected the rotor initially responds more quickly due to the centrifugal forces induced by the engine speed transient. The shroud catches up and grows more rapidly due to thermal stresses than

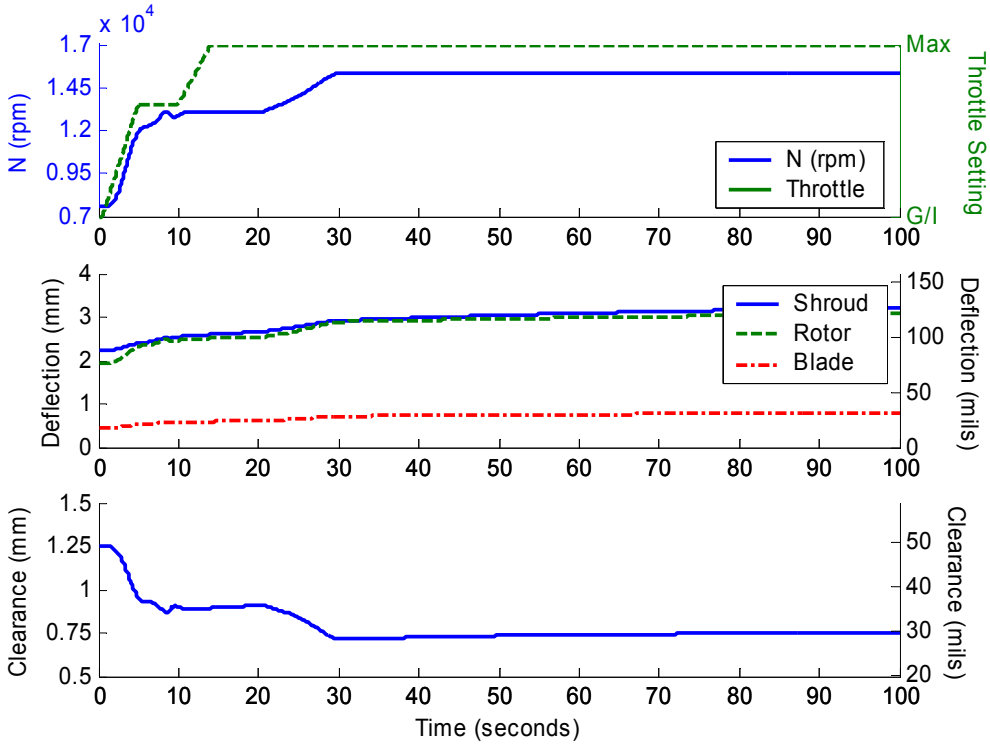

Figure 8. Deflections and clearance for lapse-rate takeoff transient

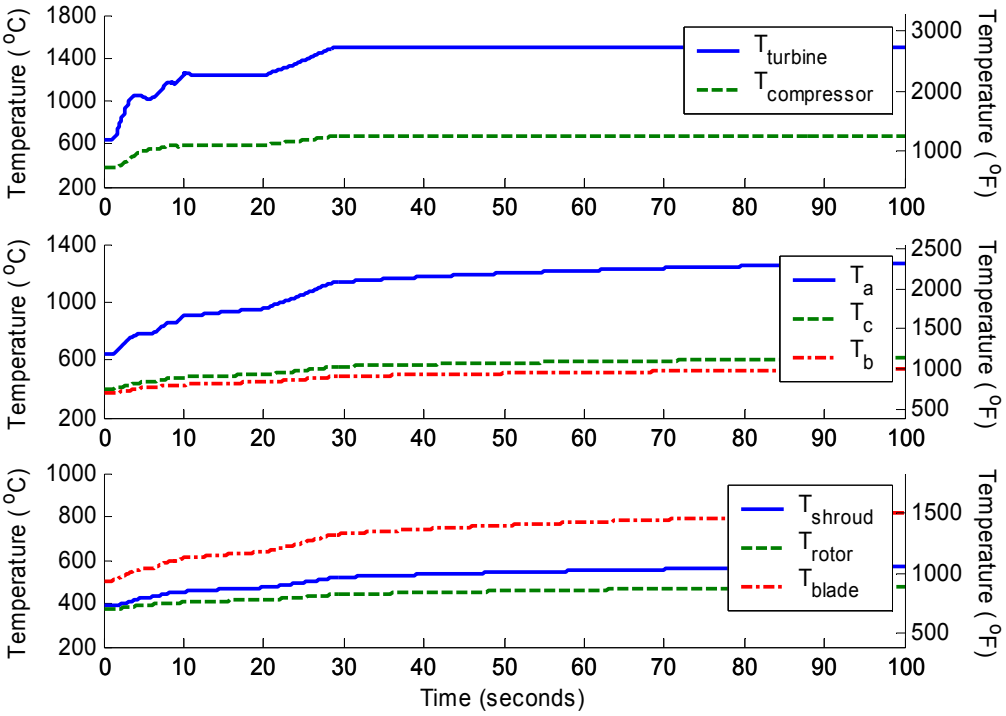

Figure 9. Temperatures for lapse-rate takeoff transient

either the rotor or blades. According to this formulation, the blades contribute the least to the clearance change. Like the rotor, they grow initially quickly due to centrifugal forces, but their growth is significantly less than the rotor which should be expected considering the relatively short length of the blades compared to the rotor radius. The predicted clearance generally follows the expected trend for a take-off-transient. The clearance is expected to reduce about 30 mils and the recovery due to the thermal growth of the shroud is expected to be about 10 mils. The model predicts a reduction of approximately 20 mils and a recovery of nearly 5 mils. Exact ranges for a given engine would depend on the parameters and transient conditions specific to that engine. Nonetheless, the results are promising. Similar comments can be made of results garnered for the lapse-rate-take-off transient (refer to Figure 8 and Figure 9).

4. Discussion

The goal of this effort is to develop a relatively simple physics-based model with sufficient accuracy for control development research. The formulation presented here, though grossly simplified, appears to reasonably predict the expected change in turbine tip clearance during a take-off-transient. Moreover, the predicted temperatures and deflection respond, for the most part, as physically expected.

Discrepancies do exist, but most deviations from expected response can likely be attributed to generalized or inaccurate information for many of the parameters used in this model. Studies by Owen [12] provide detailed information on various mechanisms effecting tip clearance, particularly with respect to the rotor and shroud. It is not the purpose of this initial model to incorporate all of the details contained therein. However, these studies provide a basis for incorporating additional details that could improve the accuracy of clearance calculation.

The true shroud thermo-mechanical response is particularly unclear, especially where interactions with the case are concerned. The turbine blades are relatively straight-forward, and, in terms of heat transfer, have been studied extensively. The blade analysis presented is, therefore, expected to be more accurate than that of the shroud or rotor. The rotor can be further complicated due to its rather non-trivial geometry and the fact that, in some gas turbines, the rotor is cooled by air at different temperatures on either of its sides.

In light of this study and the questions raised, the following tasks must be addressed to further the application and usefulness of this physics-based modeling approach:

- *Confirm materials and associated properties.* Because materials are application dependent, the material properties of Inconel 718 have been used to approximate those of various superalloys used in the manufacture turbine components. A target engine/turbine should be identified and accurate material properties used to further develop and validate this model. In particular, the abradable material must be more closely researched. The temperature dependence of many of the material properties should also be considered in future models.
- *Determine unknown convection coefficients.* The outer shroud surface and rotor surfaces are cooled by compressor discharge air and the convection process is not well documented.
- *Determine role of interaction between casing and shroud.* The shroud growth is likely limited by the casing. Documentation on casing heat transfer is not readily available.
- *Quantify roles of windage heating and heat transfer at rotor tip play in determining rotor growth.* It was assumed that the rotor temperature is primarily determined by heat transfer from cooling air discharged from the compressor. However, the effects of windage heating should be investigated as it can cause significant variation in the radial temperature distribution of the rotor. Significant heat may also be transferred from the heated blades to the circumferential tip surface of the rotor.
- *Identify thermal and mechanical response of abradable material.* The abradable material was assumed to function mostly as a thermal barrier. Its exact material properties are not known. It was assumed that the material did not respond like an alloy resulting in a thermal expansion. This assumption must be critically examined.

Future work should involve more detailed research into those parameters and mechanisms least documented. The current model should also be refined and its fidelity quantified in order to assess its usefulness for the design of a tip clearance control system. This assessment would be most meaningful if real engine data were used as a basis for comparison.

References

1. Halila, E., Lenahan, D., and Thomas, T., "Energy Efficient, High Pressure Turbine Test Hardware Detailed Design Report," NASA CR-167955, 1982.
2. Howard, W. and Fasching, W., "CF6 Jet Engine Diagnostics Program: High Pressure Turbine Roundness/Clearance Investigation," NASA CR-165581, 1982.
3. Olsson, W. and Martin, R., "B747/JT9D Flight Loads and Their Effect on Engine Running Clearance and Performance Deterioration," Nacelle Aerodynamic and Inertial Loads (NAIL)/JT9D Jet Engine Diagnostics Programs. NASA CR-165573, 1982.
4. Azad, G., Han, J., Shuye, T., and Boyle, R., "Heat transfer and pressure distributions on a gas turbine blade tip," *ASME Journal of Turbomachinery*, Vol. 122, 2000, pp. 717–724.
5. Azad, G., Han, J., and Boyle, R., "Heat transfer and flow on the squealer tip of a gas turbine blade," *ASME Journal of Turbomachinery*, Vol. 122, 2000, pp. 725–732.
6. Kim, Y., Downs, J., Soechting, F., Abdel-Messeh, W., Steuber, G., and Tanrikut, S., "A summary of the cooled turbine blade tip heat transfer and film effectiveness investigations performed by Dr. D.E. Metzger," *ASME Journal of Turbomachinery*, Vol. 117, 1995, pp. 1–11.

7. Kim, Y. and Metzger, D., "Heat transfer and effectiveness on film cooled turbine blade tip models," *ASME Journal of Turbomachinery*, Vol. 117, 1995, pp. 12–21.
8. Kumada, M., Iwata, S., Obata, M., and Watanabe, O., "Tip clearance effect on heat transfer and leakage flows on the shroud-wall surface in an axial flow turbine," *ASME Journal of Turbomachinery*, Vol. 116, 1994, pp. 39–45.
9. Lattime, S. and Steinetz, B., "Turbine engine clearance control systems: current practices and future directions," AIAA2002-3790, NASA TM-2002-211794, 38th AIAA/ASME/ASEE Joint Propulsion Conference and Exhibit, July 7-10, 2002.
10. Incropera, F. and DeWitt, D., *Fundamentals of Heat and Mass Transfer*, John Wiley & Sons, New York, NY, 1996.
11. Timoshenko, S. and Goodier, J., *Theory of Elasticity*, McGraw-Hill Book Company, New York, NY, 1970.
12. Owen, J. and Rogers, R., *Flow and Heat Transfer in Rotating Disk Systems: Volume 1 – Rotor-Stator Systems*, John Wiley & Sons Inc., New York, NY, 1989.
13. Goldstein, R., "Film cooling," *Advances in Heat Transfer*, Vol. 7, 1971, pp. 321–379.
14. Medic, G. and Durbin, P., "Toward improved prediction of heat transfer on turbine blades," *ASME Journal of Turbomachinery*, Vol. 124, 2002, pp. 187–192.
15. Medic, G. and Durbin, P., "Toward improved film cooling prediction," *ASME Journal of Turbomachinery*, Vol. 124, 2002, pp. 193–199.

Appendix

This appendix includes the Matlab© m-file and a series of block diagrams from the Simulink© model used to create the plots presented in § 3. As shown below, the m-file, `GI2MaxPower.m`, contains all parameters required for the clearance model used to produce the results. Most parameters are documented within the comments of the m-file. Input transients used in the calculations were loaded from file, `GI2MaxPower.mat`, into the Matlab© workspace. The MAT-file includes engine speed, temperature, and pressure transients used to produce the results shown in Figure 6 and Figure 7. To generate the results shown in Figure 8 and, a different MAT-file containing input transients for a lapse-rate takeoff was used. The input transients, not given here, were scaled in an attempt to make them more representative of a larger gas turbine. The Simulink© models were organized to resemble the block diagram shown in Figure 1.

GI2MaxPower.m: Matlab© m-file

```
% GI2MaxPower.m (created 071102, updated 011603/plotting)
% Turbine tip clearance parameters
% Parameter file for calculation of expansion due to
% thermal and mechanical stresses.

clear
help GI2MaxPower

% Load MAT-files
%load eng3
load GI2MaxPower            %Ground Idle to Max Power Transient

%Define Geometry, Thermal & Mechanical Properties,
% Turbine dynamic inputs
RtoK = 0.555556;            % R to K, temperature conversion
time = eng.time*2;          % slow down transient input
RPM = eng.xnh*2.45 - 21500; % increase engine speed range
t41_K = eng.t41*RtoK*0.85;  % K, turbine inlet temperature
% needed to scale compressor temperature to make sure it matched
% published temperatures for cooling air around shroud (1250 F)
t3_K  = eng.t3*RtoK*1.25;   % K, compressor discharge temperature
t41_C = t41_K - 273.15;     % C, turbine inlet temperature
t3_C  = t3_K - 273.15;      % C, turbine inlet temperature
Po = eng.p3*6894.76*0.8;    % Pa, compressor discharge pressure
Pi = (0.5/0.7)*eng.p4*6894.76;  % Pa, average turbine stage pressure
P3 = eng.p3*6894.76;        % Pa, compressor exit pressure

% Unstressed parameters
r0 = 32.9/100;              % m, rotor tip radius
L = 0.050;                  % m, blade unstressed length
Ac = 6e-4;                  % m^2, blade cross-sectional area
P = 0.110;                  % m, blade perimeter
R0 = r0+L+0.0014;            % m, thermal barrier inner radius
% Properties of Inconnel 718
rho = 8.22/1000*100^3;      % kg/m^3, density
nu = 0.4;                   % poissons ratio
c = 645;                    % J/Kg-C, specific heat
alpha1 = 15.1e-6;           % 1/K, thermal expansion coef. at 538 C
alpha2 = 16.4e-6;           % 1/K, thermal expansion coef. at 871 C
```

```
k = 24.9;                   % W/m-K, thermal conductivity at 871 C
E = 139e9;                  % Pa, modulus of elasticity at 870 C

%%%%%%%%%%%%%%%%%%%
% Shroud parameters
w = 2*0.0254;               % shroud with
a =  R0;                    % m, thermal barrier inner radius
b = a + 0.25*0.0254;        % m, shroud outer radius
rc = (a+b)/2;               % m, shroud inner radius
Aa = 2*pi*a*w;              % m^2, thermal barrier inner surface area
Ab = 2*pi*b*w;              % m^2, shroud outer surface area
V1 = pi*rc^2*w - pi*a^2*w;  % m^3, thermal barrier volume
V2 = pi*b^2*w - pi*rc^2*w;  % m^3, shroud volume
ha = 500;                   % W/m^2-K, conv. coef. thermal barrier
hb = 1000;                  % W/m^2-K, conv. coef. shroud
% Zirconium Oxide
rhoa = 5.03/1000*100^3;     % kg/m^3
ca = 0.109*4184;            % J/kg-K
ka = 2.93;                  % W/m-K
alphaa = 8.2e-6;            % 1/K, thermal expansion coef. at 1000 C
% Inconel 718
rhob = rho;                 % kg/m^3, density
cb = c;                     % J/Kg-C, specific heat
kb = k;                     % W/m-K, conductivity at 871 C
alphab = alpha1;            % 1/K, thermal expansion coef. at 538 C
% Initial conditions
Ta0 = t41_C(1);
Tb0 = t3_C(1);

%%%%%%%%%%%%%%%%%%%
% Blade parameters
V = Ac*L;                   % m^3, volume
m = rho*V;                  % kg, mass
As = L*P;                   % m^2, surface temperature
h = 1000;                   % W/m^2-K, film convection coefficient
eta = 0.5;                  % bulk film cooling effectivness
alpha = alpha2;             % 1/K, thermal expansion coef.
% Initial conditions
w0 = RPM(1)*2*pi/60;
Ti_blade = (1 -  eta)*t41_C(1) + eta*t3_C(1);

%%%%%%%%%%%%%%%%%%%
% rotor parameters
hr = 500;                   % W/m^2-K, convection coefficient
wr = w;                     % m, width
Ar = 2*pi*r0^2;             % m^2, convection surfe area
Vr = Ar*wr;                 % m^3, volume
rhor = rho;                 % kg/m^3, density
Er = E;                     % pa, modulus of elasticity
nur = nu;                   % poisson's ratio
alphar = alpha1;            % 1/K, thermal expansion coef.
cr = c;                     % J/Kg-C, specific heat
kr = k;                     % W/m-K, thermal conductivity
% Initial Condition
Trotor0 = t3_C(1);          % C, initial rotor temperature
```

```
%%%%%%%%%%%%%%%%%%
% run the simulation
[T,X,Y] = sim('ClearanceModel9',100);

RPM     = Y(:,1);
TempC   = (Y(:,2:6)-32)*5/9;   %temperature in degrees Celcius
DeflMm  = Y(:,7:9)*0.0254;     %deflections in millimeters
ClearMm = Y(:,10)*0.0254;      %clearance   in millimeters
ShTempC = (Y(:,11:15)-32)*5/9; %shroud temperatures in degrees Celcius


%%%%%%%%%%%%%%%%%%
% plot the results
set(0,'DefaultLineLineWidth',1.5)

time = [eng.time; 100]; PLA = [eng.pc; 50];

figure(1); clf
PLApcnt = 100*(PLA-21)/29;

subplot(3,1,1); [ha,h1,h2]=plotyy(T,RPM,time,PLApcnt);
    set(ha,'Xlim',[0 100]); %Common x-axis
    axes(ha(1));
        set(gca,'xgrid','off','ygrid','off','box','off');
        set(gca,'Ylim',[7000 17000],'Ytick',[7000:2500:17000]);
        ylabel('N (rpm)');
        hl=legend('N (rpm)','Throttle',0);
            hlc=get(hl,'children');
            axes(hl); ylim=get(hl,'Ylim');
            line(get(hlc(2),'Xdata'),get(hlc(2),'Ydata')-0.45*diff(ylim), ...
               'Color',get(h2,'Color'),'LineStyle',get(h2,'LineStyle'));
    axes(ha(2));
        Xlim  = get(gca,'Xlim');
        Ylim  = [0 100]; YTick = [0 100]; YTlbl = ['G/I';'Max'];
        set(gca,'xgrid','off','ygrid','off','box','off');
        set(gca,'Ylim',Ylim,'YTick',YTick,'YTickLabel',YTlbl);
        ylabel('Throttle Setting','Rotation',-
90,'VerticalAlignment','bottom');
        set(h2,'LineStyle','--');
subplot(3,1,2);
   %Left Y-Axis is metric units

    plot(T,DeflMm(:,1),T,DeflMm(:,2),'--',T,DeflMm(:,3),'-.');
    set(gca,'xgrid','off','ygrid','off','box','off');
    Ylim = get(gca,'Ylim'); YTick = Ylim(1)+diff(Ylim)*[0:0.25:1];
    set(gca,'YTick',YTick);
    ylabel('Deflection (mm)');
    hl2=legend('Shroud','Rotor','Blade');
   %Right Y-axis is English Units
    Xlim2 = get(gca,'Xlim');
    Ylim2 = get(gca,'Ylim')*(1000/25.4);
    ax2   = axes('position',get(gca,'position'));
    h2=plot(Xlim2,Ylim2,'.');  set(h2,'visible','off');
    set(ax2,'Xlim',Xlim2,'Ylim',Ylim2, ...
            'YAxisLocation','right','color','none', ...
            'xgrid','off','ygrid','off','box','off');
    ylabel('Deflection (mils)','Rotation',-90,'VerticalAlignment','bottom');
```

```
subplot(3,1,3);
   %Left Y-Axis is metric units
    plot(T,ClearMm);
    set(gca,'xgrid','off','ygrid','off','box','off');
    Ylim = get(gca,'Ylim');
    YTick = Ylim(1)+diff(Ylim)*[0:0.25:1];
    set(gca,'YTick',YTick);
    ylabel('Clearance (mm)');
    xlabel('Time (seconds)');
   %Right Y-axis is English Units
    Xlim2 = get(gca,'Xlim');
    Ylim2 = get(gca,'Ylim')*(1000/25.4);
    ax2   = axes('position',get(gca,'position'));
    h2=plot(Xlim2,Ylim2,'.');  set(h2,'visible','off');
    set(ax2,'Xlim',Xlim2,'Ylim',Ylim2, ...
            'YAxisLocation','right','color','none', ...
            'xgrid','off','ygrid','off','box','off');
    ylabel('Clearance (mils)','Rotation',-90,'VerticalAlignment','bottom');
print -depsc2 -tiff GI2MPdeflections;
print -dmeta GI2MPdeflections;

figure(gcf+1); clf
set(gcf,'position',get(gcf-1,'position').*[1.05 0.96 1 1]);
subplot(3,1,1);
   %Left Y-Axis is metric units
    plot(T,TempC(:,1),T,TempC(:,2),'--');
    set(gca,'xgrid','off','ygrid','off','box','off');
    Xlim  = [  0  100];
    Ylim  = [200 1800];
    YTick = Ylim(1):400:Ylim(2);
    set(gca,'Xlim',Xlim,'Ylim',Ylim,'YTick',YTick);
    ylabel('Temperature ( ^oC)');
    legend('T_{turbine}','T_{compressor}');
   %Right Y-axis is English Units
    Xlim2 = get(gca,'Xlim');
    Ylim2 = get(gca,'Ylim')*(9/5)+32;
    ax2   = axes('position',get(gca,'position'));
    h2=plot(Xlim2,Ylim2,'.');  set(h2,'visible','off');
    set(ax2,'Xlim',Xlim2,'Ylim',Ylim2, ...
            'YAxisLocation','right','color','none', ...
            'xgrid','off','ygrid','off','box','off');
    ylabel('Temperature ( ^oF)','Rotation',-90,'VerticalAlignment','bottom');
subplot(3,1,2);
   %Left Y-Axis is metric units
    plot(T,ShTempC(:,2),T,ShTempC(:,3),'--',T,ShTempC(:,4),'-.');
    set(gca,'xgrid','off','ygrid','off','box','off');
    Xlim  = [  0  100];
    Ylim  = [200 1400];
    YTick = Ylim(1):400:Ylim(2);
    set(gca,'Xlim',Xlim,'Ylim',Ylim,'YTick',YTick);
    ylabel('Temperature ( ^oC)');
    legend('T_a','T_c','T_b');
   %Right Y-axis is English Units
    Xlim2 = get(gca,'Xlim');
    Ylim2 = get(gca,'Ylim')*(9/5)+32;
    ax2   = axes('position',get(gca,'position'));
    h2=plot(Xlim2,Ylim2,'.');  set(h2,'visible','off');
```

```
    set(ax2,'Xlim',Xlim2,'Ylim',Ylim2, ...
            'YAxisLocation','right','color','none', ...
            'xgrid','off','ygrid','off','box','off');
    ylabel('Temperature ( ^oF)','Rotation',-90,'VerticalAlignment','bottom');
subplot(3,1,3);
   %Left Y-Axis is metric units
    plot(T,TempC(:,3),T,TempC(:,4),'--',T,TempC(:,5),'-.');
    set(gca,'xgrid','off','ygrid','off','box','off');
    Xlim  = [  0  100];
    Ylim  = [200  1000];
    YTick = Ylim(1):200:Ylim(2);
    set(gca,'Xlim',Xlim,'Ylim',Ylim,'YTick',YTick);
    ylabel('Temperature ( ^oC)');
    xlabel('Time (seconds)');
    legend('T_{shroud}','T_{rotor}','T_{blade}');
   %Right Y-axis is English Units
    Xlim2 = get(gca,'Xlim');
    Ylim2 = get(gca,'Ylim')*(9/5)+32;
    ax2   = axes('position',get(gca,'position'));
    h2=plot(Xlim2,Ylim2,'.');  set(h2,'visible','off');
    set(ax2,'Xlim',Xlim2,'Ylim',Ylim2, ...
            'YAxisLocation','right','color','none', ...
            'xgrid','off','ygrid','off','box','off');
    ylabel('Temperature ( ^oF)','Rotation',-90,'VerticalAlignment','bottom');
print -depsc2 -tiff GI2MPtemperatures;
print -dmeta GI2MPtemperatures;

figure(gcf-1);
```

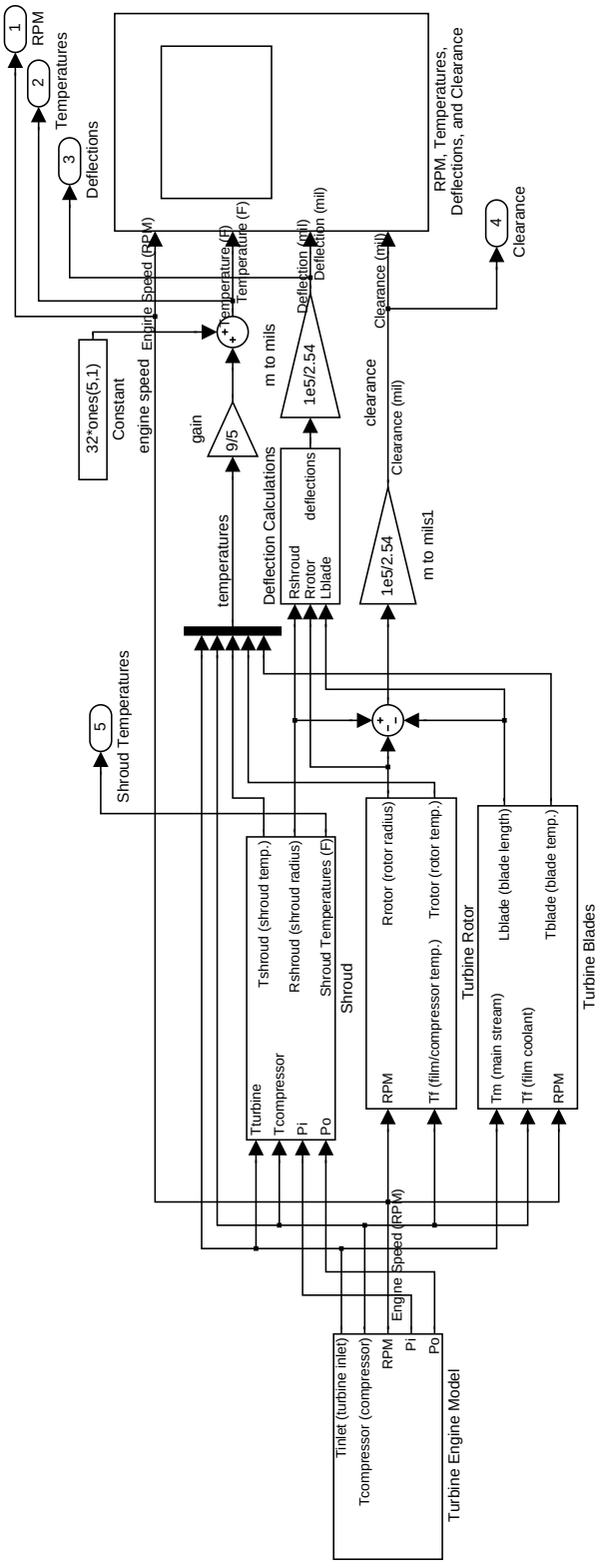

Figure A-1. Simulink© block diagram of TipClearance Model

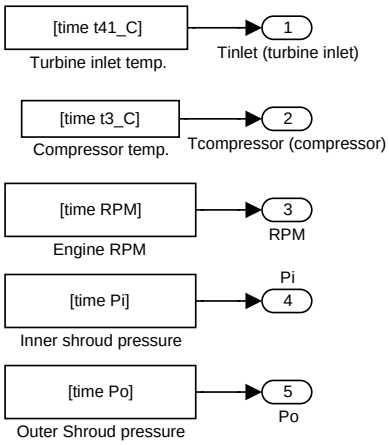

Figure A-2. Engine sub-model

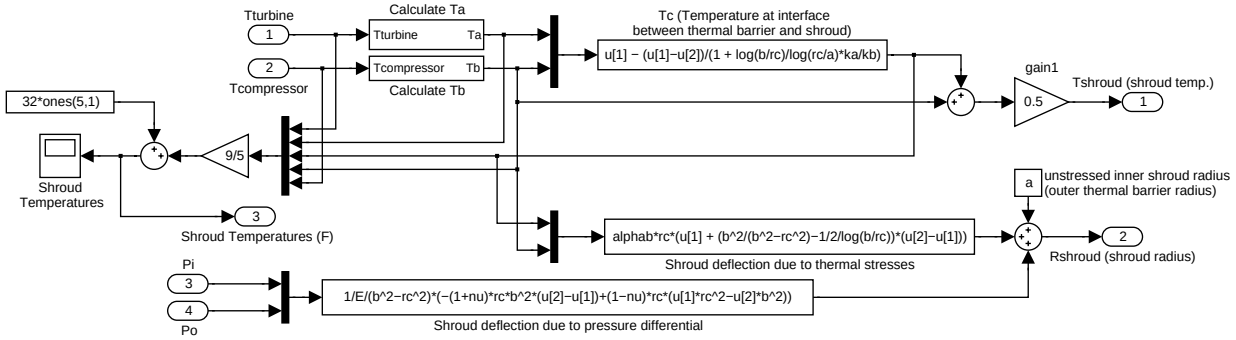

Figure A-3. Shroud sub-model

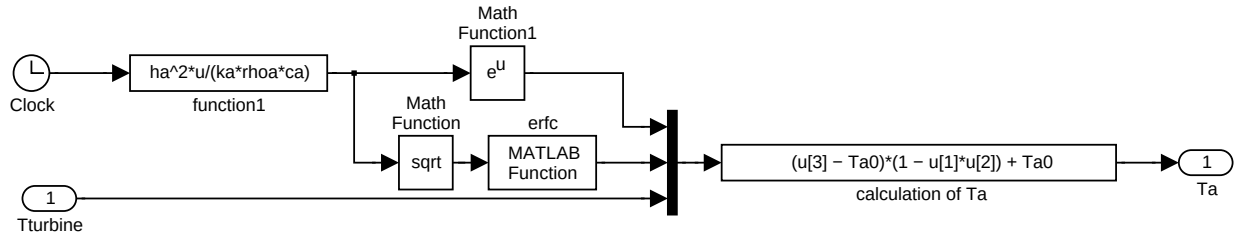

Figure A-4. Inner shroud surface temperature, T_a, sub-model

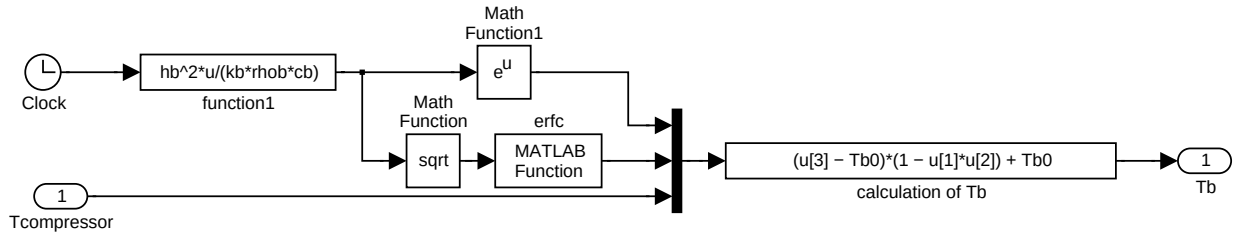

Figure A-5. Outer shroud surface temperature, T_b, sub-model

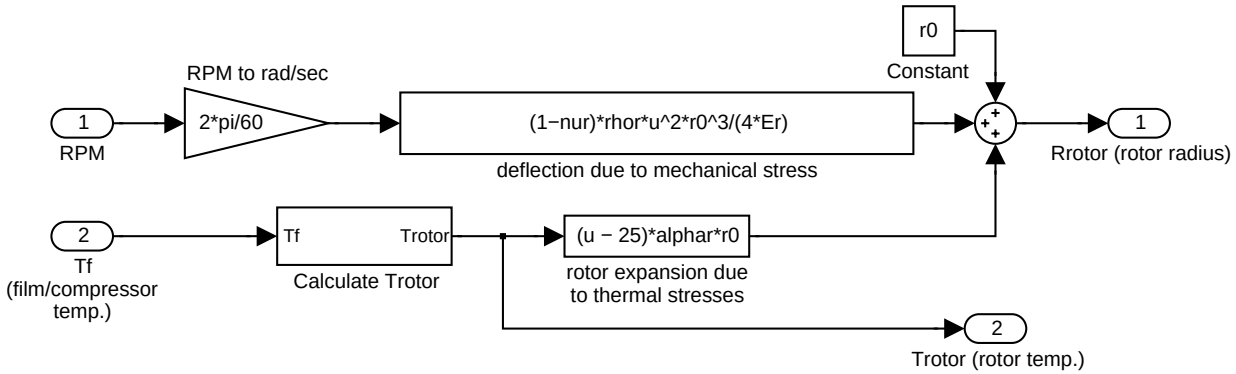

Figure A-6. Rotor sub-model

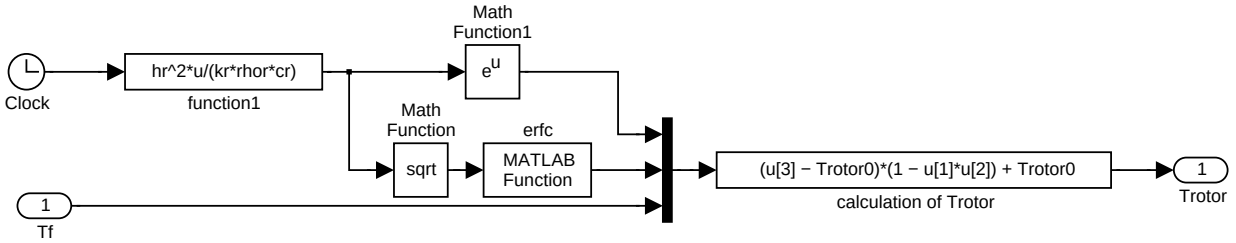

Figure A-7. Rotor surface temperature, T_{rotor}, sub-model

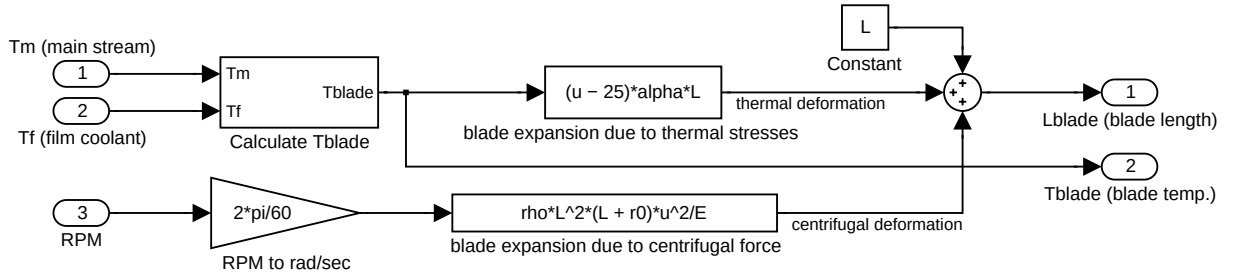

Figure A-8. Blade sub-model

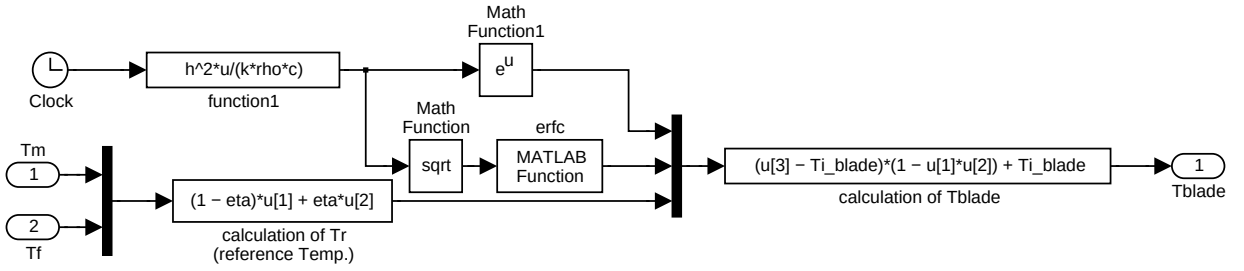

Figure A-9. Blade surface temperature, T_{blade}, sub-model

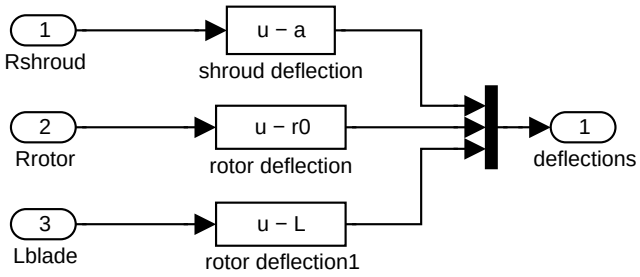

Figure A-10. Deflection calculations sub-model

REPORT DOCUMENTATION PAGE

Form Approved
OMB No. 0704-0188

1. AGENCY USE ONLY (*Leave blank*)	2. REPORT DATE	3. REPORT TYPE AND DATES COVERED
	March 2003	Technical Memorandum

4. TITLE AND SUBTITLE

A Reduced Model for Prediction of Thermal and Rotational Effects on Turbine Tip Clearance

5. FUNDING NUMBERS

WBS–22–708–87–06

6. AUTHOR(S)

Javier A. Kypuros and Kevin J. Melcher

7. PERFORMING ORGANIZATION NAME(S) AND ADDRESS(ES)

National Aeronautics and Space Administration
John H. Glenn Research Center at Lewis Field
Cleveland, Ohio 44135–3191

8. PERFORMING ORGANIZATION REPORT NUMBER

E–13846

9. SPONSORING/MONITORING AGENCY NAME(S) AND ADDRESS(ES)

National Aeronautics and Space Administration
Washington, DC 20546–0001

10. SPONSORING/MONITORING AGENCY REPORT NUMBER

NASA TM—2003-212226

11. SUPPLEMENTARY NOTES

Javier A. Kypuros, University of Texas, Pan American University, Edinburg, Texas 78539; Kevin J. Melcher, NASA Glenn Research Center. Responsible person, Kevin J. Melcher, organization code 5530, 216–433–3743.

12a. DISTRIBUTION/AVAILABILITY STATEMENT

Unclassified - Unlimited
Subject Category: 07 Distribution: Nonstandard

Available electronically at http://gltrs.grc.nasa.gov

This publication is available from the NASA Center for AeroSpace Information, 301–621–0390.

12b. DISTRIBUTION CODE

13. ABSTRACT ***(Maximum 200 words)***

This paper describes a dynamic model that was developed to predict changes in turbine tip clearance—the radial distance between the end of a turbine blade and the abradable tip seal. The clearance is estimated by using a first principles approach to model the thermal and mechanical effects of engine operating conditions on the turbine subcomponents. These effects are summed to determine the resulting clearance. The model is demonstrated via a ground idle to maximum power transient and a lapse-rate takeoff transient. Results show the model demonstrates the expected "pinch point" behavior. The paper concludes by identifying knowledge gaps and suggesting additional research to improve the model.

14. SUBJECT TERMS

Clearances; Active control; Turbine

15. NUMBER OF PAGES

32

16. PRICE CODE

17. SECURITY CLASSIFICATION OF REPORT	18. SECURITY CLASSIFICATION OF THIS PAGE	19. SECURITY CLASSIFICATION OF ABSTRACT	20. LIMITATION OF ABSTRACT
Unclassified	Unclassified	Unclassified	